Electron-Impact Excitation and Ionization in Air

Winifred M. Huo
Huo Consulting LLC, Los Altos, CA 94024-3168 USA

Winifred.M.Huo@nasa.gov, w.m.huo@sbcglobal.net

ABSTRACT

In a partially ionized hypersonic flow field, electron collision plays a significant role in energy re-distribution and in the production of excited states of atoms and molecules that can subsequently radiate. Thus electron collision data is part of the database used in modelling high speed entry flows. First principles computational methods for the calculation of electron-impact data are reviewed. Their merits are discussed, based on the requirements of reliability and the ability to handle high-lying excited states. Three processes are considered: the production of electrons by electron-impact ionization, the removal of electrons by radiative recombination and dielectronic recombination, and the production of electronic excited states by electron impact. Electron-nitrogen atom collisions are used as an illustrative example. The study clarifies the role of high-lying electronic excited states in the ionization process. It shows that the recombination processes can produce sizable radiative heat load in the VUV region. It also shows examples using a scaling method to improve the frequently used Born approximation for electron-impact excitations.

1.0 INTRODUCTION

During the hypersonic entry of a space vehicle into a planetary or lunar atmosphere, the flow field becomes partially ionized. The percentage of ionization depends on the entry speed and the vehicle size. In this regime, electron collision provides an efficient means of producing electronic excited states of the atoms and molecules in the flow field. Thus it plays an important role in determining the internal energy and state distribution of the gaseous particles. The excited states in turn are the source of radiation observed during a hypersonic entry.

Electron-atom/molecule collisions differ from heavy particle (atom-atom, atom-molecule and molecule-molecule) collisions in two aspects. First, the mass of an electron is more than four orders of magnitude smaller than the reduced mass of N_2. Thus its average speed, and hence its average collision frequency, is more than 100 times larger. Even in the slightly ionized regime with only 1% electrons, the frequency of electron-atom/molecule collisions is equal to or larger than that of heavy particle collisions, an important consideration in the low density part of the atmosphere where the reaction probability is frequently controlled by the collision frequency. Second, the interaction potential between a charged particle (electron) and a neutral particle is longer range than neutral-neutral interactions. Hence electron-atom/molecule collision cross sections tend to be larger. Also, low-energy electron collisions can be effective in spin changing excitations. Another characteristic of electron collisions is that it generally produces a variety of excited states whereas heavy particle collisions tend to produce specific excited states.

Modelling electron collisions in nonequilibrium gas dynamics requires data to simulate its production and removal in the flow field. Also, in the non-equilibrium regime where the populations of radiative species are

Report Documentation Page

Form Approved
OMB No. 0704-0188

1. REPORT DATE	2. REPORT TYPE	3. DATES COVERED
SEP 2009	**N/A**	**-**

4. TITLE AND SUBTITLE
Electron-Impact Excitation and Ionization in Air

5a. CONTRACT NUMBER
5b. GRANT NUMBER
5c. PROGRAM ELEMENT NUMBER

6. AUTHOR(S)

5d. PROJECT NUMBER
5e. TASK NUMBER
5f. WORK UNIT NUMBER

7. PERFORMING ORGANIZATION NAME(S) AND ADDRESS(ES)
Huo Consulting LLC, Los Altos, CA 94024-3168 USA

8. PERFORMING ORGANIZATION REPORT NUMBER

9. SPONSORING/MONITORING AGENCY NAME(S) AND ADDRESS(ES)

10. SPONSOR/MONITOR'S ACRONYM(S)
11. SPONSOR/MONITOR'S REPORT NUMBER(S)

12. DISTRIBUTION/AVAILABILITY STATEMENT
Approved for public release, distribution unlimited

13. SUPPLEMENTARY NOTES
See also ADA562449. RTO-EN-AVT-162, Non-Equilibrium Gas Dynamics - From Physical Models to Hypersonic Flights (Dynamique des gaz non- equilibres - Des modeles physiques jusqu'au vol hypersonique)., The original document contains color images.

14. ABSTRACT
In a partially ionized hypersonic flow field, electron collision plays a significant role in energy re-distribution and in the production of excited states of atoms and molecules that can subsequently radiate. Thus electron collision data is part of the database used in modelling high speed entry flows. First principles computational methods for the calculation of electron-impact data are reviewed. Their merits are discussed, based on the requirements of reliability and the ability to handle high-lying excited states. Three processes are considered: the production of electrons by electron-impact ionization, the removal of electrons by radiative recombination and dielectronic recombination, and the production of electronic excited states by electron impact. Electron-nitrogen atom collisions are used as an illustrative example. The study clarifies the role of high-lying electronic excited states in the ionization process. It shows that the recombination processes can produce sizable radiative heat load in the VUV region. It also shows examples using a scaling method to improve the frequently used Born approximation for electron-impact excitations.

15. SUBJECT TERMS

16. SECURITY CLASSIFICATION OF:			17. LIMITATION OF ABSTRACT	18. NUMBER OF PAGES	19a. NAME OF RESPONSIBLE PERSON
a. REPORT	b. ABSTRACT	c. THIS PAGE			
unclassified	**unclassified**	**unclassified**	**SAR**	**22**	

determined by the quasi-steady-state approximation, the electron number density, temperature, and electron-impact excitation rate coefficients are part of the input data for QSS calculation. Similar data needs also exist in other disciplines dealing with plasma, including astrophysics, fusion science, plasma processing in microelectronics, etc. While the composition and temperature of the plasmas may be different, these communities frequently employ a common set of approximate formulas for the cross section/rate coefficient expressions. Using a combination of experimental data and a variety of approximate formulas, a number of databases have been developed in the entry physics community. The data sets by Park [1,2], Losev [3] and Bird's TCE [4,5] models are well established examples of this approach. The NEQAIR package [6] that simulates nonequilibrium radiation in an entry flow employs Gryzinski's [7] classical formula is used for electron-impact excitation of atoms whereas for molecules experimental data are used, sometimes by extrapolation or by analogy. More recent models have incorporated improved databases, based on new experimental data and/or theoretical calculations. The collisional radiative model by Bourdon et al. [8] includes many updates. Similarly SPRADIAN07 [9] incorporated new, improved data into the NEQAIR model.

As part of a systematic development of a physics-based model of nonequilibrium chemistry and radiation in hypersonic flow, it is timely to investigate and update the electron collision cross-sections/rate coefficients based on first principles calculations. The present focus is on electron-atom collisions, because atomic radiation dominates at high entry speed. Our study covers electron-impact ionization. Together with associative ionization, they are the production mechanisms of electrons in the flow field. Two electron removal mechanisms are investigated, radiative recombination and dielectronic recombination. Selected electron-impact excitations of bound-bound transitions are also studied.

2.0 QUANTUM MECHANICAL FORMULATION OF ELECTRON COLLISIONS

Due to the light electron mass, in general e-atom/molecule collisions should be treated using quantum mechanics instead of classical mechanics. The Schrödinger equation for an e-atom system is given by

$$(H-E)\Psi(\tau_1 \text{L}\ \tau_{N+1}) = 0 \tag{1}$$

Here H is the Hamiltonian of the e + atom system, E the total energy, Ψ the corresponding wave function, and τ_i the spatial and spin coordinates of the i^{th} electron. The indices i and j label the bound electrons, and $N+1$ label the free electron. Due the large difference between electron and nuclear mass, it is assumed that the nucleus is fixed during the collision. The total Hamiltonian consists of the atomic Hamiltonian, H_A, the kinetic energy operator of the free electron, $\mathcal{T}_e$, and the Coulomb potential V between the free electron and the atom.

$$H = H_A + \mathcal{T}_e + V, \tag{2}$$

$$H_A = -\frac{1}{2}\sum_{i=1}^{N}\nabla_i^2 + \sum_{i>j}^{N}\frac{1}{|\mathbf{r}_i - \mathbf{r}_j|} - \sum_{i=1}^{N}\frac{Z}{|\mathbf{r}_i|}, \tag{3}$$

$$\mathcal{T}_e = -\frac{1}{2}\nabla_{N+1}, \tag{4}$$

$$V = \sum_{i}^{N} \frac{1}{|\mathbf{r}_{N+1} - \mathbf{r}_i|} - \frac{Z}{|\mathbf{r}_{N+1}|}. \tag{5}$$

Here Z is the nuclear charge. The origin of the coordinate system is chosen to be at the nucleus.

The solution to Eq. (1) are obtained by first solving the atomic Schrödinger equation.

$$(H_A - E_A)\Phi(\tau_1 \text{L } \tau_N) = 0. \tag{6}$$

In the range of incident electron energy of interest to hypersonic flow modelling, from threshold to ≈100 eV, the close coupling method [10] provides the most reliable solution of Eq. (1).

$$\Psi(\tau_1 \text{L } \tau_{N+1}) = \sum_{m=0}^{\infty} \mathcal{A}\{f_m(\tau_{N+1})\Phi_m(\tau_1 \text{L } \tau_N)\}. \tag{7}$$

The antisymmetrizer $\mathcal{A}$ permutes the free electron with the bound electrons to account for the fact that electrons are indistinguishable and must satisfy Fermi statistics. The summation is over all possible states of the atom, including the continuum. The summation in Eq. (7) becomes integration in the continuum region. The excitation/ionization cross section is obtained by analyzing the asymptotic behavior of the function f_m. Because there are an infinite number of discrete and continuum target states, for practical reasons the summation is necessarily truncated. The success of a close coupling calculation depends on the quality of the atomic wave functions used and the number of terms included in the summation. Two of the most successful approaches used in e-atom collisions are the convergent close-coupling (CCC) method [11, 12, 13] and the R-matrix with pseudo states (RMPS) [14,15]. In the CCC method expands target states using square-integrable functions. The convergence of such representation is tested by successively increasing the size of the basis. While the CCC method has demonstrated excellent results, so far its application is limited to atoms/ions with one or two electrons outside a closed shell core, i.e., the alkali and alkaline earth atoms. The current version is not applicable to N, O, and their ions that exist in the Earth entry environment. The RMPS method is an extension of the R-matrix method [16]. The target functions used in the Eq. (7) are constructed using both physical orbitals determined from the solution of Eq. (6) and pseudo orbitals constructed using a Sturmian-type basis or B-spline. The latter approximately represent the high-lying bound states and continuum states. This method is applicable to atoms/ions of arbitrary structure, but the accuracy of the calculation depends on the number of physical target states used in the expansion.

Simulation of nonequilibrium gas dynamics requires a complete set of cross sections involving all possible initial and final states of the atom/molecule. The NIST database [18] lists 381 levels for N atom not counting the high Rydberg states. Thus a very large set of cross-section data are needed. As discussed in the preceding paragraph, modern quantum mechanical calculations can provide reliable cross data but the accurate calculations are limited to a small set of low-lying states for a given atom, or applied only to a particular class of atoms. Therefore it is necessary to employ approximate methods. The most frequently employed approximations are classical mechanics or Born approximation based on screened hydrogenic target functions. Both are attractive to modellers of macroscopic phenomena because analytic formulas are available, making the calculation of large numbers of cross sections feasible. At present the best practice is to use experimental or more accurate quantal treatment when available, and supplement the data set using either the classical or the hydrogenic approximations.

It is difficult to predict *a priori*, under what conditions these approximation will fail. As an example, consider a calculation of Li atom using three different types of target wave functions, screened hydrogenic, Hartree-Fock (HF) [17], and Multiconfiguration Hartree-Fock (MCHF) [17] functions. In the HF method, the electron sees the averaged potential from other electrons and the atomic wave function is an antisymmetrized product of one-electron orbitals (one-electron solution of the Fock equation). Electron correlation arising from instantaneous electron-electron interaction is neglected. The MCHF method accounts for electron correlation approximately by expanding the wave function in terms configuration state functions, i.e, antisymmetrized products one-electron orbitals. The ground state of Li has the electronic configuration $1s^2 2s\ ^2S$ and the electronic configuration of the first excited state is $1s^2 2p\ ^2P$. Since the 1s electrons are more tightly bound than the 2s or 2p electron, the screened hydrogenic approximation should apply well to these states. Table 1 presents selected properties calculated using these wave functions and experimental data when available. For the expectation value of r of the 2s orbital, $\langle \phi_{2S} | r | \phi_{2S} \rangle$, all three methods are in good agreement with each other. For the Einstein A coefficient of the $^2S - {}^2P$ transition, $A_{2S,2P,}$ the HF and MCHF results are in good agreement with NIST tabulation [18], but $A_{2S,2P}$ calculated using screened hydrogenic functions is ≈ a factor of 5 smaller. The electron-impact excitation cross section for the $^2S - {}^2P$ transition is calculated at 4 eV incident electron energy using both the Born approximation [19] and the BE scaling method [20]. The cross section recommended by Wutte et al [21] based on a compilation of experimental data is also presented. The BE scaling cross sections calculated using with MCHF and HF wave functions are in good agreement with experiment, with the MCHF result slightly closer to experiment. The Born cross sections are approximately a factor of 3 larger. On the other hand, the Born cross section from the screened hydrogenic calculation is in excellent agreement with experiment, whereas the BE scaling result is a factor of 3 smaller. However, based on the fact that the screened hydrogenic calculation gives a poor result for $A_{2S,2P}$, the good agreement in the Born cross section is due to fortuitous cancelations of errors in which the screened hydrogenic approximation underestimates and the Born approximation overestimates the cross section.

Table 1: Comparison of properties of Li atom using screened hydrogenic, HF, and MCHF wave functions

Property	Screened hydrogenic	HF	MCHF	Experiment
$\langle \phi_{2S} \| r \| \phi_{2S} \rangle$ (au)	4.00	3.87	3.86	
$A_{2S,\,2P}$ (s^{-1})	6.63E+06[a]	3.75E+07[a]	3.87E+07	3.72E+07[b]
$\sigma_{2S\text{-}2P}$ ($Å^2$)[c], Born	36.6	117.8	106.6	36.6[d]
$\sigma_{2S\text{-}2P}$ ($Å^2$)[c], BE	12.7	39.7	37.9	36.6[d]

[a]Photon wavelength is determined from MCHF calculation.
[b]NIST data [18].
[c]4 eV incident electron energy.
[d]Critical compilation by Wutte et al [21].

The Li atom example serves to illustrate two requirements for reliable transition properties, high quality atomic wave functions and a treatment of collision dynamics that is applicable to low energies**.** In the present application, the MCHF method is used. Since the study is limited to light atoms, relativistic effects are treated

by solving the Breit-Pauli Hamiltonian [17]. The collision dynamics treatment used in the study of ionization and excitation is described below.

2.1 Electron-impact ionization

There are two mechanisms in electron-impact ionization. The first is direct ionization where the colliding electron directly detaches a bound electron from the atom or molecule.

$$A + e \rightarrow A^{+} + 2e. \tag{8}$$

The second mechanism is autoionization. It is an indirect process where the atom is first excited to a bound electronic state that lies in the continuum. The bound state is sufficiently energetic that it automatically ionizes.

$$A + e \rightarrow A^{*} \rightarrow A^{+} + 2e. \tag{9}$$

The total ionization cross section is the sum of the two contributions.

$$\sigma_I = \sigma_{DI} + \sigma_{AI}\,. \tag{10}$$

The cross term between direct and autoionization has been neglected. Different methods are used to calculate direct ionization and autoionization cross sections.

2.1.1 Direct ionization

Quantum theory has a demonstrated record of successful calculations of the total ionization cross-sections by electron impact [22]. The Binary-Encounter-Dipole (BED) model of electron-impact ionization developed by Kim and Rudd [23] has been used for a large variety of atoms and molecules and the BED cross-sections are available in the NIST database [24]. The improved Binary-Encounter-Dipole (iBED) model [25] was introduced in 2001 to improve the treatment of the dipole term in the BED model. In the iBED model, the direct ionization cross section is expressed in two terms,

$$\sigma_{DI} = \sigma_{BinaryEncounter} + \sigma_{BornDipole} \tag{11}$$

The Binary-Encounter cross-section $\sigma_{BinaryEncounter}$ describes the close collision between the free electron and bound electron. It is represented by a modified Mott cross-section with the incident electron energy replaced by the average energy from the Binary-Encounter model [26]. The dipole Born cross section accounts for the long range interaction between the free electron and the target. The difference between the iBED and BED models lies in the use of the Dipole Born cross-section instead of the Dipole Bethe cross-section. The former includes the effect of electron shielding, thus improving the description of the process at low incident electron energies. The formula for σ_{DI} used in this study is given in Ref. 25, Eq. (2.46). All parameters used in the calculation are obtained using *ab initio* calculations.

2.1.2 Autoionization

Autoionization is a two-step process. The initial state of the atom, *i*, is first excited to a metastable state, *m*. The latter decays either by ionization or by radiative decay. Thus the autoionization cross section is given by the product of the electron impact excitation cross section σ_{im} and the ionization probability of the metastable state, P_m^I.

$$\sigma_{AI} = P_m^I \sigma_{im}. \tag{12}$$

The ionization probability is given by

$$P_m^I = \frac{k_{I,m}}{k_{I,m} + k_{R,m}}, \tag{13}$$

with $k_{I,m}$ and $k_{R,m}$ the ionization and radiative rate coefficients of state *m*. The electron-impact excitation cross section σ_{im} is calculated using the BE scaling method [20] discussed in Sec. 2.2.

2.2 Electron-impact excitation

The Born approximation [19] is the most commonly used method for the calculation of electron-impact excitation cross sections. It is based on a perturbation series expansion of the transition matrix element,

$$T_{if} = \left\langle e^{i\mathbf{k}_f \bullet \mathbf{r}_{N+1}} \Phi_f(\mathbf{r}_1 \ldots \mathbf{r}_N) \middle| V + VG_o^{(+)}V + VG_o^{(+)}VG_o^{(+)}V + \ldots \middle| e^{i\mathbf{k}_i \bullet \mathbf{r}_{N+1}} \Phi_i(\mathbf{r}_1 \ldots \mathbf{r}_N) \right\rangle. \tag{14}$$

$$G_o^{(+)} = (E - H_o + i\delta)^{-1}, \tag{15}$$

$$H_o = H_A + \mathcal{T}_e. \tag{16}$$

δ is a small positive number. The first term in Eq. (14) is the Born term. The series converges when the interaction potential *V* is significantly smaller than the incident electron energy. Thus the Born approximation is a high energy approximation. The Born cross section is given by

$$\sigma_{if}^{Born} = \frac{4\pi}{k_i^2} \int_{K_{\min}^2}^{K_{\max}^2} \frac{1}{K^4} \left| \left\langle \Phi_f(\tau_1 \ldots \tau_N) \middle| \sum_{l=1}^{N} e^{i\mathbf{K}\bullet\mathbf{r}_l} \middle| \Phi_f(\tau_1 \ldots \tau_N) \right\rangle \right|^2 dK^2. \tag{17}$$

The momentum transfer $\boldsymbol{K}$ is given by $\boldsymbol{K} = \boldsymbol{k_i} - \boldsymbol{k_f}$, with $\boldsymbol{k}_i$ and $\boldsymbol{k_f}$ the momentum vector of the incident and scattered electron. For hydrogenic functions, the Born cross section is given in closed form.

The energy regime of interest in modelling hypersonic flow is too low for the Born approximation to hold. The Born approximation, while describing long range interaction such as dipole and quadrupole interaction well, does not account for electron exchange, the polarization of the target electrons by the free electron, and the distortion of the free electron by the target that are described by higher order terms in the perturbation series. The BE scaling method by Kim [20] incorporates these effects approximately by energy scaling.

$$\sigma_{if}^{BE} = \sigma_{if}^{Born}\left(\frac{E_e}{E_e + B + E_x}\right). \quad (18)$$

Here E_e is the free electron energy. B is the ionization energy of the initial state, i.e., the binding energy of the outermost electron. E_x is the excitation energy. The BE scaling method has been used successfully in treating electron collisions with neutral atoms and ions [20,27]. For ionic target, the plane wave in Eq. (14) is replaced by a Coulomb wave. It should be noted that this method does not include resonance effects, that is, the enhancement of the collision cross section due to the formation of transient compound states. Resonances should be treated separately. The BE scaling method is used in the present study of electron-impact excitation and autoionization.

3.0 ELECTRON-IMPACT IONIZATIN OF N ATOM

Ionization from ten states of N atom is studied. Their electronic structures and ionization potentials are presented in Table 2. The first three states share the ground state electronic configuration, $1s^2 2s^2 2p^3$. The upper seven states has one electron in the n=3 shell.

Table 2: Electronic structure and ionization potentials of 10 states of N atom used in the ionization calculation

Electronic configuration	Ionization potential (eV)	Electronic configuration	Ionization potential (eV)
$1s^2 2s^2 2p^3\ {}^4S^o$	14.534	$1s^2 2s^2 2p^2({}^3P)3s\ {}^2P$	3.854
$1s^2 2s^2 2p^3\ {}^2D^o$	12.151	$1s^2 2s^2 2p^2({}^3P)3p\ {}^4D^o$	2.784
$1s^2 2s^2 2p^3\ {}^2P^o$	10.959	$1s^2 2s^2 2p^2({}^3P)3p\ {}^4P^o$	2.697
$1s^2 2s^2 2p^2({}^3P)3s\ {}^4P$	4.208	$1s^2 2s^2 2p^2({}^3P)3d\ {}^4F$	1.557
$1s^2 2s^2 2p^2({}^1D)3s\ {}^2D$	4.076	$1s^2 2s^2 2p^2({}^3P)3d\ {}^4D$	1.518

The cross section calculations use atomic wave functions calculated using the ATSP2K code [28]. For the metastable $^2D^o$ and $^2P^0$ states, the autoionizaton rate coefficients are taken from Kim and Desclaux [29]. Results for the three lowest states have been reported previously [30].

Figure 1 compares the calculated cross section with the cross-beam experiment of Brook et al [31]. The composition of the N atom beam used in the experiment has been analyzed by Kim and Desclaux [29] to be approximately 70% $^4S^0$ and 30% $^2D^0$. Figure 1 presents the calculated electron-impact ionization cross section for such mixture of N atoms and compares with experiment. The reported experimental error is ± 40% at low

energies and ± 15% at higher energies. As seen in the Figure, the calculated cross sections agree with experiment to within their error estimate.

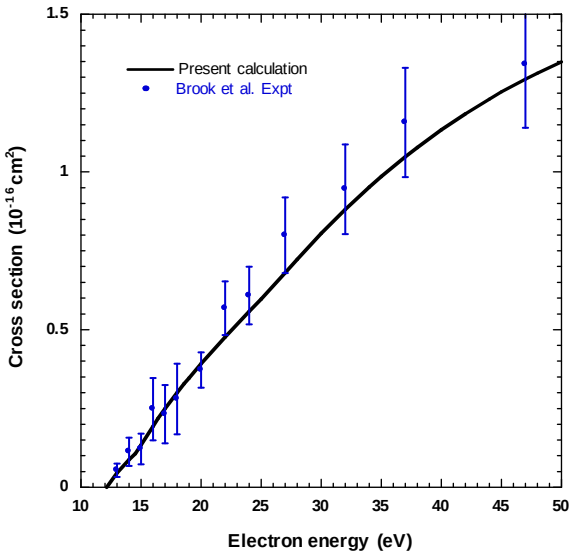

Figure 1. Ionization cross-section as a function of free electron energy for a mixture of N atoms composed of 70% $^4S^0$ and 30% $^2D^0$. Experimental data are from Brook et al [31].

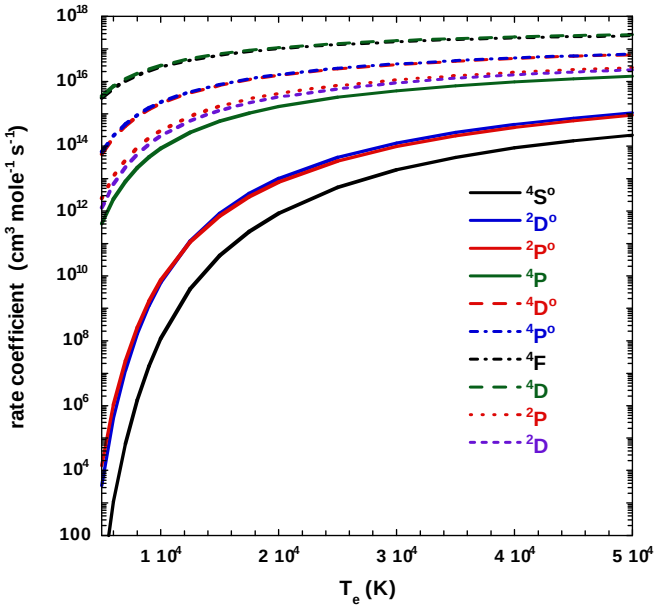

Figure 2. Ionization rate coefficients for 10 states of N atom as a function of free electron temperature.

The ionization rate coefficients from 10 states of N are presented in Figure 2. It is seen that the rate coefficients separate into two groups. The three lowest states, being more tightly bound, have smaller ionization rates than the seven states that has one electron in the n=3 shell. The difference is particularly striking at low electron temperatures. The large ionization rates of the upper states lends to the possibility that the upper states will first reach Saha equilibrium with the free electron before they reach Boltzmann equilibrium with the lower states.

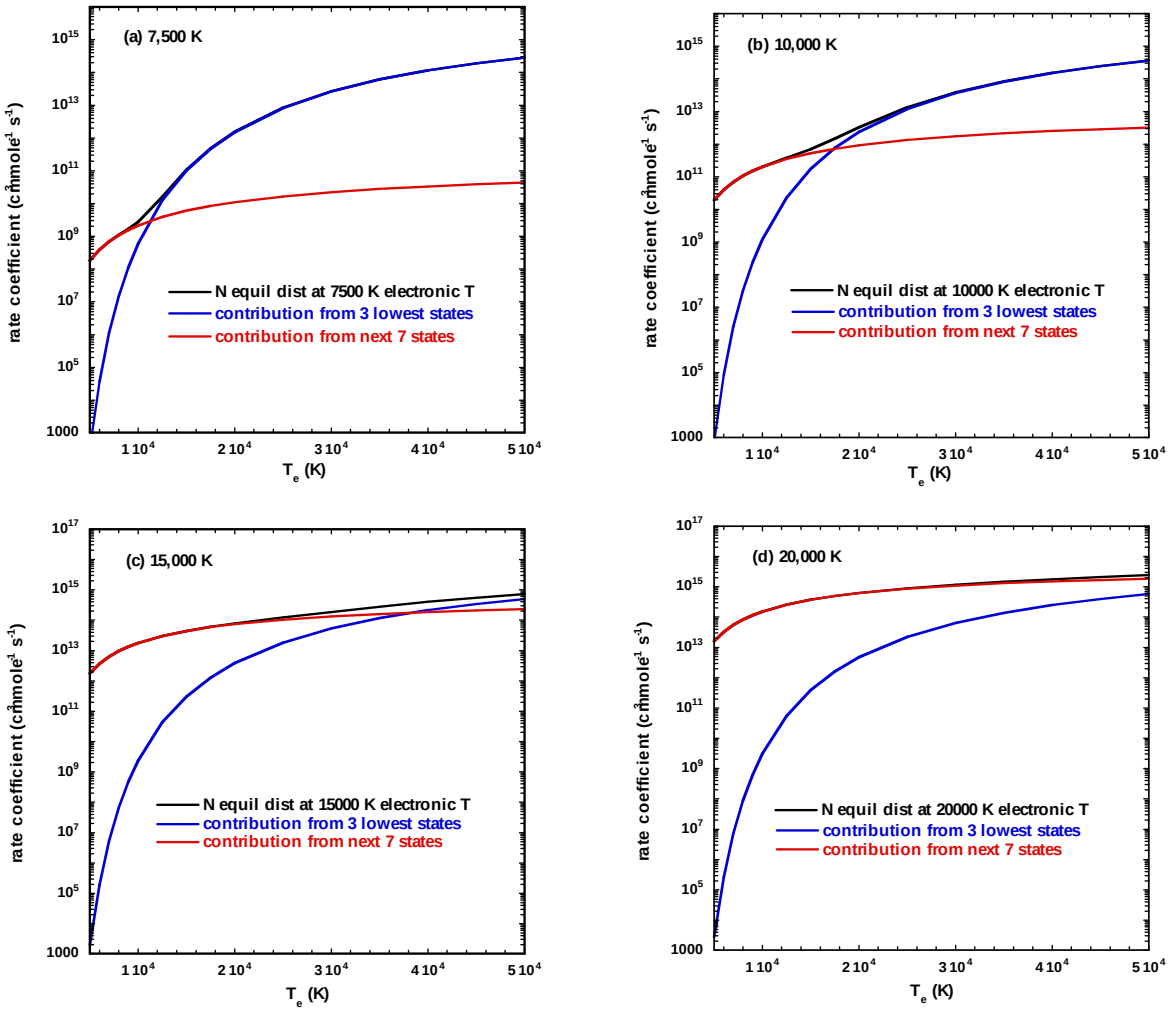

Figure 3. Boltzmann ionization rate coefficients of N atom as a function of free electron temperature. 10 electronic states of N atom are used in the Boltzmann calculation. The electronic temperature of the atom is (a) 7,500 K, (b) 10,000 K, (c) 15,000 K and (d) 20,000 K. The contributions from the 3 lowest states and the 7 upper states are also presented.

Since most CFD simulations employ a single ionization rate coefficient for each species, Boltzmann rate coefficients calculated using a Boltzmann distribution of the 10 states at 7,500, 10,000, 15,000 and 20,000 K electronic temperatures are presented in Figures 3 a - d. The calculation neglects the remaining upper states of

the atom and separates the internal electronic temperature of the atom from the free electron temperature. Also shown are the contributions from the 3 lowest states and the 7 upper states. At 7,500 and 10,000 K, the Boltzmann rate is determined from the ionization of the upper states at low T_e, but determined by the lower state rates at T_e larger than the internal electronic temperature of the atom. At 15,000 – 20,000 K, the Boltzmann rate is determined by the upper state rates. Note that under hypersonic entry conditions, the upper states are likely not to be Boltzmann equilibrium with the 3 lowest states and their number densities are likely to be orders of magnitude smaller than the Boltzmann distribution. Instead, the upper states are in Saha equilibrium with the free electron. The FIRE II analysis by Panesi et al. [32] provides a good illustration of this situation. Thus a single ionization rate for each species, as presented in Fig. 3 for N atom, most likely is not a good approximation.

4.0 ELECTRON RECOMBINATION WITH N^+ ION

There are two types of electron-ion recombination processes, radiative recombination (RR) and dielectronic recombination (DR). In both cases the focus of the present study is in the radiance produced by the recombination because both RR and DR can be a significant source of radiative power.

4.1 Radiative recombination

In radiative recombination, the electron recombines with an ion and a photon is emitted.

$$N^+(n'l's') + e \rightarrow N(nls) + h\nu. \tag{19}$$

It is the reverse of photoionization. The photon energy emitted in RR is given by

$$h\nu = E_{N^+} - E_N + E_e. \tag{20}$$

The process is illustrated schematically in Figure 4. Because the electron energy is continuous, the radiation emitted is also continuous.

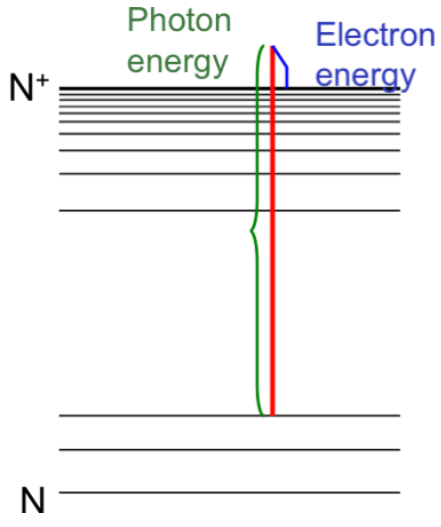

Figure 4. Schematic diagram of radiative recombination.

The radiative power produced by RR is given by [33],

$$\left\langle \frac{d(h\nu)}{dt} \right\rangle = \frac{2}{\sqrt{\pi}} N_e \overline{\upsilon}_e \int_0^\infty \varepsilon h\nu \sigma_{n'l's'-nls}(\varepsilon) \exp(-\varepsilon) d\varepsilon. \tag{21}$$

Here $\varepsilon = E_e/k_B T_e$ is the electron energy scaled by $k_B T_e$. In terms of the photon wavelength Eq. (21) is rewritten as

$$\left\langle \frac{d(h\nu)}{dt} \right\rangle = N_e \overline{\upsilon}_e \frac{2hc}{\sqrt{\pi} k_B T_e} \int_0^\infty \varepsilon h\nu \sigma_{n'l's'-nls}(\varepsilon) \exp(-\varepsilon) \lambda^{-2} d\lambda. \tag{22}$$

Thus the radiance R produced at wavelength λ by the RR of A^+ ions in the ($n'l's'$) state to all neutral states is

$$R(\lambda) = (2\pi^{3/2}\lambda^3 k_B T_e)^{-1} h^2 c^2 N_{ion} N_e \overline{\upsilon}_e \sum_{nls} \varepsilon \sigma_{n'l's'-nls}(\varepsilon) \exp(-\varepsilon). \tag{23}$$

The total radiance R_{total} is obtained by integrating over the photon wavelength

$$R_{total} = \int_0^\infty R(\lambda) d\lambda. \tag{24}$$

The RR rate coefficients tabulated in the literature [34, 35] is related to the RR cross-section by

$$k_{n'l's-nls}(T_e) = \frac{2}{\sqrt{\pi}} \overline{\upsilon}_e \int_0^\infty \varepsilon \sigma_{n'l's'-nls}(\varepsilon) \exp(-\varepsilon) d\varepsilon. \tag{25}$$

The average RR cross-section [33] is related to the rate coefficient by

$$\sigma_{n'l's'-nls}(E_e) \approx \left\langle \sigma_{n'l's'-nls}(T_e) \right\rangle = \int_0^\infty \varepsilon \sigma_{n'l's'-nls}(\varepsilon) \exp(-\varepsilon) d\varepsilon = \frac{\sqrt{\pi}}{2} \frac{k_{n'l's'-nls}(T_e)}{\overline{\upsilon}_e}. \tag{26}$$

The AMDPP website [34] provides RR rate coefficients of N^+ recombined to form neutral N states up to n = 8 and l = 7. Under the *ls* coupling scheme, the calculation covers 4 ion states and 406 neutral states. Under *jj* coupling, there are 6 ion states and 1052 neutral states. Temperature covered ranges from 10 – 10,000,000 K. Nahar and Pradhan [35] also reported RR data of N^+. They cover recombination to 20 neutral states, with highest n = 4, l = 3. Temperature range is 100 – 10,000 K. Only one ion state is covered. In the present calculation, we choose to use the AMDPP database because it covers four ion states in *ls* coupling. Two modifications were made to the AMDPP database. First, the energy levels of N and N^+ in the AMDPP database were determined using approximate quantum mechanical calculations. For most states, there are significant differences between the AMDPP values versus the NIST data [18]. Hence all energy levels in the AMDPP database are replaced by the NIST data when possible. Scaling is used when the corresponding data are not available. The second modification is to extend the number of neutral states that are formed by the recombination of the ground ($^3P^o$) state of N^+. We generate additional 176 N levels from n=9 to 12 and l=0 to 7. The RR rate coefficients for the additional states are assumed to be the same as n=8 levels.

The calculation [30] uses the parameters T_e = 10,460 K, N_e = 1.19×10^{16} cm^{-3}, and N_{N+} = 1.02×10^{16} cm^{-3}. It covers wavelengths from 10 nm to 10,000 nm. The radiance from the four N^+ states are weighed by the Boltzmann factor and summed. The electronic temperature of N^+ is assumed to be the same as the free electron temperature. The calculated radiance spectrum can be divided into three regions.

(1) 120 – 10,000 nm. In this region, the RR spectrum is low-intensity, continuous and rather structureless, a typical background spectrum.

(2) 50 – 120 nm. Here the radiance spectrum is significantly more intense, as shown in Fig. 5(a). It consists of a series of very sharp peaks, with a sharp, precipitous rise on the long wavelength side and a slower decrease on the short wavelength side. The onset of the sharp peaks are at 113.09, 101.97, 88.15, 85.25 nm. The maximum radiance in this region, at 85.25 nm, is 512.6 W cm^{-3} μm^{-1} sr^{-1}. By comparison, the maximum radiance in the 120-1000 nm region is 0.5 W cm^{-3} μm^{-1} sr^{-1}, approximately three orders of magnitude smaller. The large radiance and the continuous nature of the spectrum make this important contribution to the radiative heat flux. To better understand the peak structure, Figure 5(b) shows the individual contribution from the four ion states, without the Boltzmann weight factor. The RR of the ground state ion shows three peaks, from recombination to the lowest three neutral states, $2s^2 2p^3\ ^4S^o$, $^2D^o$, and $^2P^o$. The RR of the $^1D^o$ ion has two peaks, from recombination to the $2s^2 2p^3\ ^2D^o$ and $^2P^o$ states of N. The RR of the $^1S^o$ ion has one peak for recombination to the $2s^2 2p^3\ ^2P^o$ state of N. The RR of the $^5S^o$ ion has two peaks from recombination to the $2s^2 2p^3\ ^4S^o$ and $2s2p^4\ ^4P$ of N. The sharp onset of each peak is characteristic of the RR process. As seen in Figure 5(b), the maximum of RR occurs at threshold electron energy, after which the rate goes down with electron energy. This is reflected in the decrease of radiance at the short wavelength side of the peak.

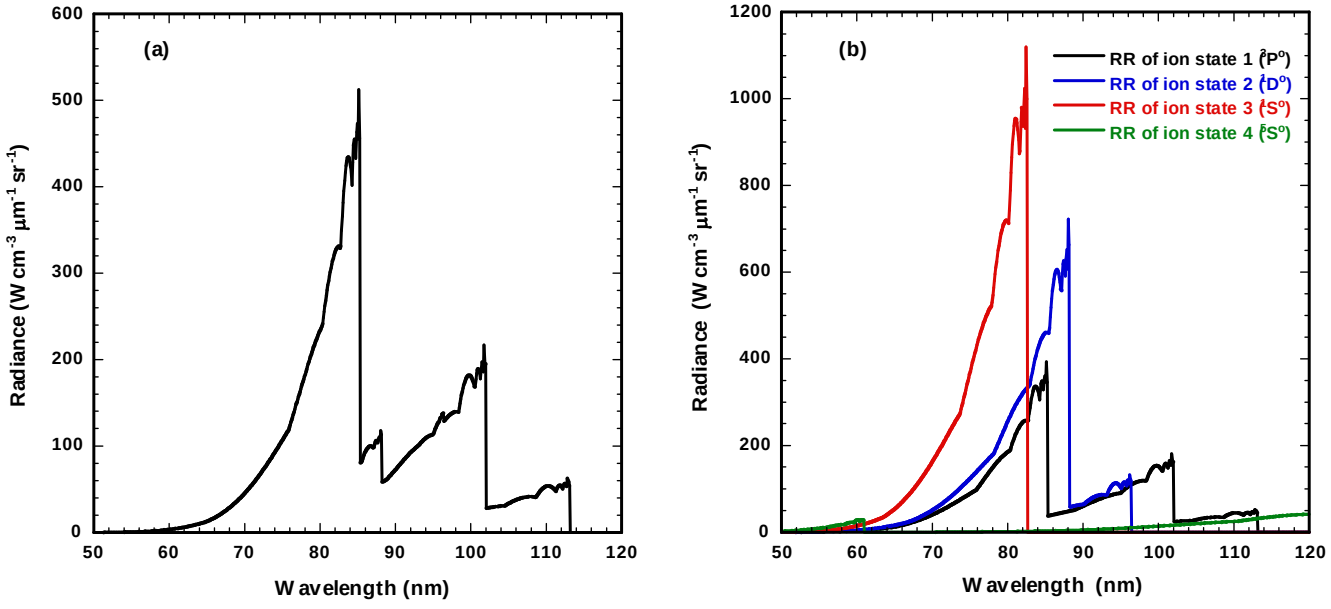

Figure 5. (a) Radiance spectrum from RR of N^+ in the 50 – 120 nm region. (b) Radiance spectrum from the RR of four lowest N^+ states.

(3) 10 – 50 nm. The radiance spectrum in this region is extremely weak. Increasing the number of ion state used in the calculation may improve the spectrum. However, the higher-lying ion state has a small Boltzmann weight factor. Therefore they will not change the results in a meaningful way.

4.2 Dielectronic recombination

In dielectronic recombination, the electron recombines with an ion and produces a metastable, excited state of the neutral. The metastable state can either emits an electron and goes back to the ion (Auger process) or emits a photon and decays to a lower state.

$$A^+(n'l's') + e \leftrightarrow A^*(n^*l^*s^*) \rightarrow A(nls) + h\nu. \tag{27}$$

$$h\nu = E_{A^*} - E_A. \tag{28}$$

$$E_e = E_{A^*} - E_A. \tag{29}$$

The emitted photon is from a bound-bound transition. Thus dielectronic recombination produces a discrete spectrum. A schematic diagram of dielectronic recombination is shown in Figure 6.

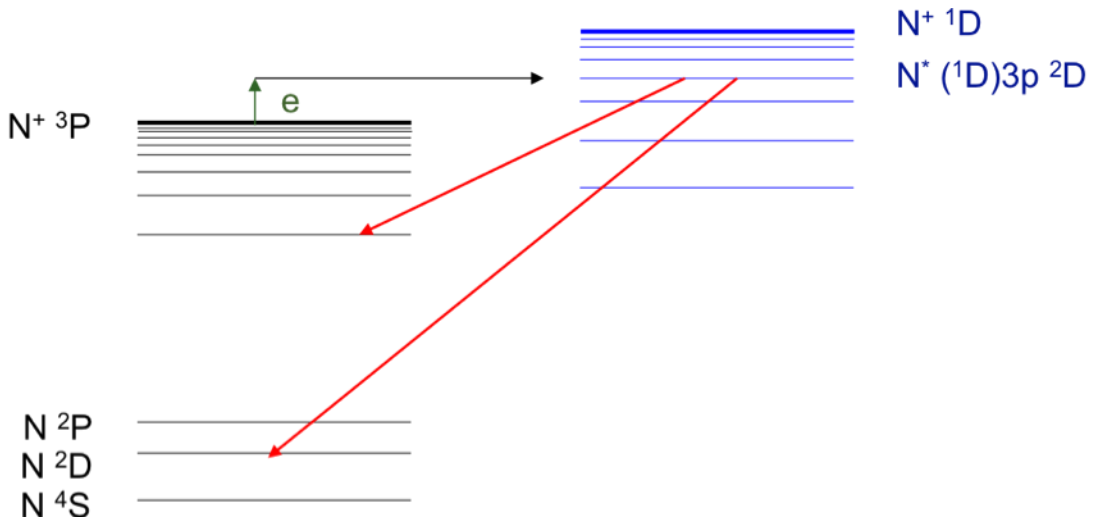

Figure 6. Schematic diagram of dielectronic recombination.

The radiance R at wavelength λ produced by all dielectronic recombination processes is given by

$$R(\lambda) = (2\pi^{3/2}\lambda^3 k_B T_e)^{-1} h^2 c^2 N_{ion} N_e \overline{\upsilon}_e \sum_{nls} \varepsilon \sigma^{DR}{}_{n'l's'-nls}(\varepsilon) \exp(-\varepsilon). \tag{30}$$

The dielectronic recombination cross section $\sigma^{DR}{}_{n'l's'-nls}$ from ion state (*n'l's'*) to form a neutral state (*nls*) is given by

$$\sigma^{DR}_{n'l's'-nls} = \frac{\pi}{2E_e}\sum_i \frac{g_{N_i^*}}{2g_{N^+}} \frac{1}{(E_N - E_{N_i^*})^2 - (\Gamma_{N_i^*}/2)^2} A_a^{N_i^* N^+} A_r^{N_i^* N}. \quad (31)$$

Here the summation is over all metastable states N_i^* that participates in the recombination process.

The dielectronic recombination of N^+ has been studied at T_e = 10460 K, N_e = 1.19×10^{16}cm^{-3} and N_{N+} = 1.02×10^{16}cm^{-3}. The metastable excited states N^* used in the calculations are the series of states that converge to the $2s^22p^2(^1D)$ state of N^+: $2s^22p^2(^1D)4s\ ^2D$, $2s^22p^2(^1D)3d\ ^2F$, $2s^22p^2(^1D)3d\ ^2D$, and $2s^22p^2(^1D)3d\ ^2P$. The Auger rate coefficients in the cross section calculation are from the AMDPP database [36] and the radiative rate coefficients are from the NIST database [18].

Figure 7a compares the total radiance from DR and RR in the 98 – 112 nm region. The different characteristics of the two recombination processes are clearly evident. Except for the sharp threshold due to the onset of the recombination of the ground state $N^+(^3P^o)$ to the $N(^2D^o)$ state at 102 nm, the RR spectrum is a continuum spectrum. The DR spectrum, on the other hand, is composed of sharp peaks typical of bound-bound transitions. This is in accordance with the physics of DR recombination where radiation is emitted from the bound, metastable state of the neutral atom, N^*, to a lower bound state. At the sharp peaks in the DR spectrum, the RR spectrum is lower in intensity by a couple orders of magnitude or more. However, the continuum character of the RR spectrum means the total radiance from RR is significant. Indeed, in the VUV region, 50 – 120 nm, the two contributions are comparable: the total RR radiance is 6.50 W cm^{-3} sr^{-1} whereas the DR radiance is 7.28 W cm^{-3} sr^{-1}. In the visible and near infrared region, the contributions from both processes drop significantly. For example, in the 1000 – 1500 nm region, the total radiance from DR is 0.14 W cm^{-3}sr^{-1}. An example of the DR spectrum in the infrared region is presented in Figure 7b. In this region, the RR spectrum is too weak to be discernable.

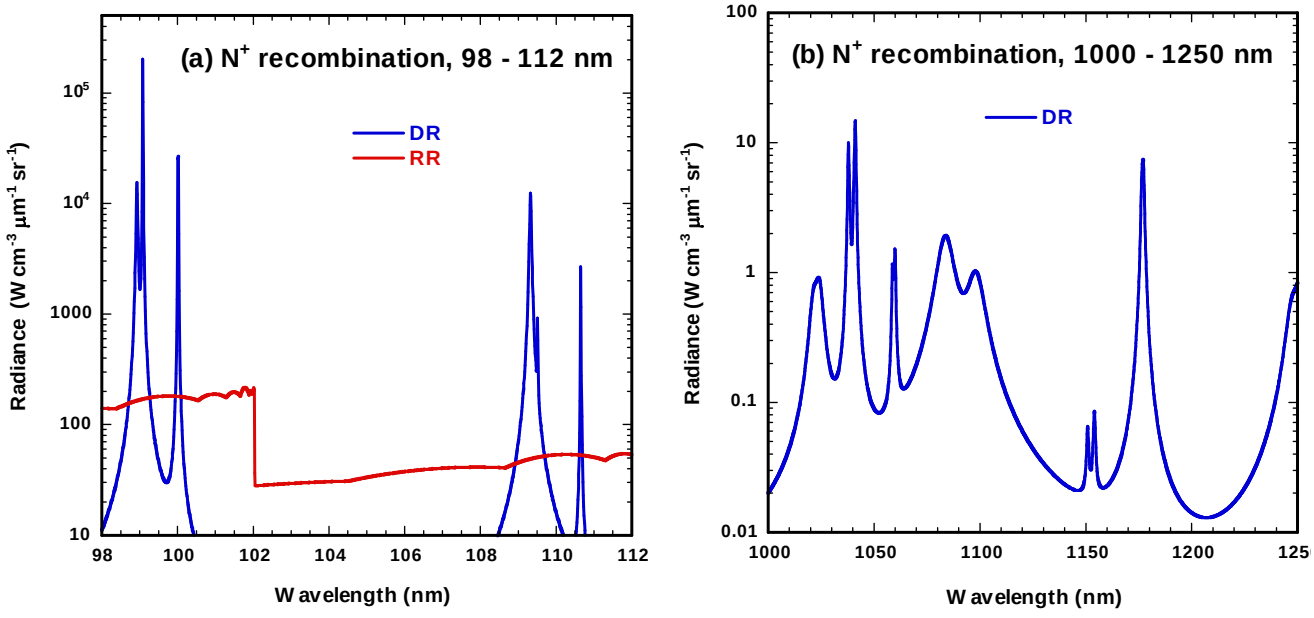

Figure 7. (a) Radiance spectrum from DR and RR of N^+ in the 98 – 112 nm region. (b) Radiance spectrum from the DR of N^+ in the 1000 – 1250 nm region. RR spectrum is not discernable in this region.

5.0 ELECTRON-IMPACT EXCITATION OF N ATOM

Experimental data of electron-impact excitation of N atom is sparse. Measurements of excitation cross section from the ground $^4S^o$ to $1s^2 2s^2 2p^2(^3P)3s\ ^4P$ have been reported by Spence and Burrow [37] and by Doering and Goembel [38]. Spence and Burrow [37] and Doering and Goembel [39] reported cross section measurements for the $^4S^o$ to $1s^2 2s2p^4\ ^4P$ transition, and Yang and Doering [40] measured cross sections for the $^4S^o$ to $^2D^o$ transition. A number of R-matrix calculations have been reported for the e-N system, but so far no RMPS calculations have been carried out. Tayal and Beatty [41] reported a study of the $^4S^o$ to $^2D^o$ excitation in an 11-state close coupling approximation using the R-matrix method. Frost et al. [42] carried out a 33-term close coupling calculation using the R-matrix method and determined collision strengths from the 3 lowest states to 21 states with $n \leq 3$. They also reported experimental rate coefficients determined using spectroscopic measurements in an arc chamber. Comparison between calculation and experiment shows agreement for some transitions and deviations in others.

As discussed in Sec. 2, quantal treatments based on the close coupling formulation using high-level atomic wave functions are not yet available to cover high-lying excited states, such as nitrogen with one electron in the $n \geq 4$ shell. The BE scaling method is considered a possible alternative approach because it retains the simplicity of the Born approximation but included higher order effects not covered in the Born approximation by a scaling method. Figure 8 presents cross sections for the $1s^2 2s^2 2p^3\ ^2P^o$ – $1s^2 2s2p^4\ ^2S$ transition calculated using both the Born and the BE scaling method. MCHF atomic wave functions determined using the ATSP2K code are used. Since the ^2S state lies above the first ionization limit, it has not been treated by the R matrix method. Experimental data is also not available. It is seen from Fig. 8 that the Born cross section is significantly larger than the BE scaling cross section at low energies because the lack of polarization and distortion effects in the Born treatment. Note also that the Born cross sections in Fig. 8 are calculated using MCHF wave functions. Further deviation will be found if hydrogenic wave functions are used.

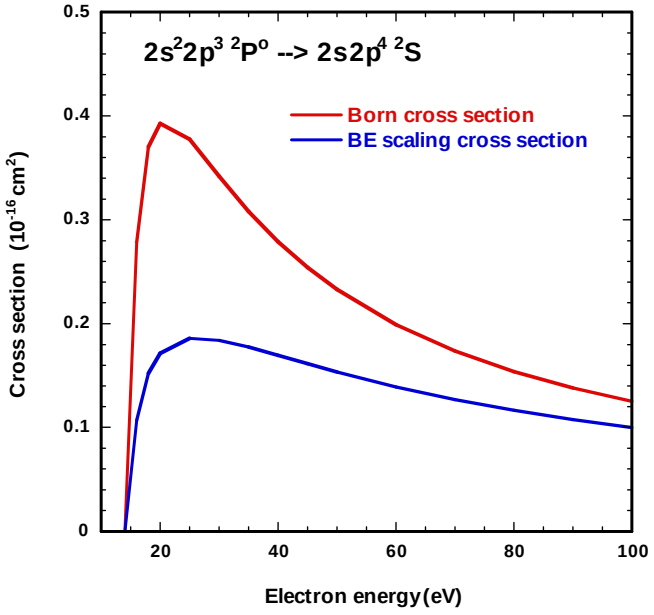

Figure 8. Electron-impact excitation cross section for the $1s^2 2s^2 2p^3\ ^2P^o$ – $1s^2 2s2p^4\ ^2S$ transition of N atom calculated using the Born approximation and the BE scaling method.

6.0 CONCLUSION

In this study we have investigated quantum mechanical calculations of electron-collision data with the purpose of generating a database for modeling hypersonic entry flow. A major difficulty encountered is that simulations of nonequilibrium gas dynamics require a complete set of cross sections involving all possible initial and final states of the atom whereas modern quantum mechanical calculations can provide accurate cross section data only for a small set of low-lying states of an atom, or applied only to a particular class of atoms. Thus a major goal of this study is to investigate approximate methods that not only can extend the database beyond what is currently available from experiments or R-matrix calculations, but also can provide better quality data than the Born approximation or classical mechanics treatment used in many current databases. Electron-nitrogen atom collisions are used as an example. For ionization, a combination of the iBED method for direct ionization, and BE scaling method for autoionization provides ionization cross sections of N atom in good agreement with experimental data for the low-lying states. The method is then used to calculate the ionization cross sections for higher-lying states. It is seen that the ionization rate coefficients for individual states separate into two groups. The three lowest states, being more tightly bound, have smaller ionization rates than the seven states that has one electron in the n=3 shell. The difference is particularly striking at low electron temperature. The large ionization rates of the upper states lend credence to the possibility that the upper states will first reach Saha equilibrium with the free electron before they reach Boltzmann equilibrium with the lower states. It is likely that, under such circumstances, a single ionization rate for each species, such as commonly used in CFD modeling, may not be adequate. For electron recombination, the radiance from radiative recombination and dielectronic recombination of N^+ is investigated, based on the rate coefficients from the AMDPP database. These two processes contribute significantly to the radiative heat load in the VUV region, a region not easily accessible in experiment. For electron-impact excitation, the cross section for the $1s^22s^22p^3\ ^2P^o - 1s^22s2p^4\ ^2S$ transition of nitrogen is used to illustrate the difference between the Born approximation and BE scaling method. A large difference is found in the low energy region important in modelling hypersonic flows. This is ascribed to the lack of polarization and distortion effects in the Born treatment. Thus the BE scaling method should offer a better description of the excitation process.

7.0 ACKNOWLEDGMENTS

This work is funded by NASA/ARMD Fundamental Aeronauics/Hypersonics Program contract # NNA07BA89C.

8.0 NOMENCLATURE

A = neutral atom or molecule
A^+ = ion
$A_a^{N^*N+}$ = Auger rate coefficient for the autoionization of a metastable state
A_{ki} = Einstein A coefficient
$A_r^{N^*N}$ = radiative rate coefficient of a metastable state ($n^*l^*s^*$) to the final state (nls)
c = speed of light

CCC = convergent close-coupling method for e-atom collisions
DR = dielectronic recombination
e = electron
E = total energy of the electron + atom system
E_A = energy of atom in (nls) state
E_{A+} = energy of ion in ($n'l's'$) state
E_{A*} = energy of atom in metastable ($n^*l^*s^*$) state
E_e = free electron energy
E_{IP} = ionization energy of atom in (nls) state
E_N = energy of nitrogen atom in (nls) state
E_{N*} = energy of nitrogen atom in metastable ($n^*l^*s^*$) state
E_{N+} = energy of nitrogen ion in ($n'l's'$) state
E_x = excitation energy
f_m = free electron function associated with the m^{th} state of the atom in a close coupling calculation
F = cumulative fraction of integrated radiation intensity
$G_o^{(+)}$ = Green's function
g_{N*} = degeneracy factor of the metastable state
g_{N+} = degeneracy factor of the ion
h = Planck's constant
H = Hamiltonian
H_A = Hamiltonian of the atom
H_o = Hamiltonian of the atom plus electron, without interaction
HF = Hartree-Fock method
$\boldsymbol{K}$ = momentum transfer vector of the free electron
k_B = Boltzmann constant
$\boldsymbol{k}_f$ = momentum vector of the scattered electron
$\boldsymbol{k}_i$ = momentum vector of the incident electron
k_I = electron-impact ionization rate coefficient
$k_{I,m}$ = electron-impact ionization rate coefficient of state m
$k_{n'l's'\text{-}nls}$ = radiative recombination rate coefficient of ion in ($n'l's'$) state to neutral in (nls) state
$k_{R,m}$ = radiative decay rate coefficient of state m
l = angular momentum quantum number of neutral atom
l^* = angular momentum quantum number of neutral atom in a metastable state
l' = angular momentum quantum number of ion
MCHF = Multiconfiguration Hartree-Fock method
n = principal quantum number of neutral atom
n^* = principal quantum number of neutral atom in a metastable state
n' = principal quantum number of ion
N = nitrogen atom
N^* = nitrogen atom in a metastable state
N_i^* = the i^{th} metastable state of nitrogen atom
N^+ = nitrogen ion
N_e = electron number density
N_{ion} = ion number density
N_{N+} = nitrogen ion number density
P_m^I = ionization probability of the metastable state m
QSS = quasi-steady state approximation
R = radiance

R_{total} = total radiance
RMPS = R-matrix with pseudo states method for electron-atom collisions
RR = radiative recombination
s = spin quantum number of neutral atom
s^* = spin quantum number of neutral atom in a metastable state
s' = spin quantum number of ion
t = time
T_e = electron temperature
T_{if} = transition matrix between atomic state i and f
$\mathcal{T}_e$ = kinetic energy operator of the free electron
V = Coulomb interaction potential between the free electron and the atom
$\bar{v}_e$ = average electron velocity
δ = a small positive number
ε = scaled electron energy
Φ = atomic wave function
ϕ = one-electron orbital
λ = photon wavelength
ν = photon frequency
σ_I = electron-impact ionization cross-section
σ_{DI} = direct electron-impact ionization cross-section
σ_{AI} = autoionization cross-section
$\sigma_{BinaryEncounter}$ = Binary-Encounter cross-section
$\sigma_{DipoleBborn}$ = Dipole Born cross-section
$\sigma_{n'l's'\rightarrow nls}$ = radiative recombination cross-section of ion in (*n'l's'*) state to neutral in (*nls)* state
$\langle\sigma_{n'l's'\rightarrow nls}\rangle$ = average radiative recombination cross-section of ion in (*n'l's'*) state to neutral in (*nls)* state
$\sigma^{DR}{}_{n'l's'-nls}$ = dielectronic recombination cross section from ion state (*n'l's'*) to neutral state (*nls*)
τ = Spatial and spin coordinates of the electron
Ψ = Wave function of the electron + atom system.
∇^2 = Laplacian operator

9.0 REFERENCES

[1] PARK, C. "Review of Chemical-Kinetic Problems of Future NASA Missions I. Earth Entries," *J. Thermophysics and Heat Transfer* Vol. 7**,** 385-398 (1993).

[2] PARK, C. Jaffe, R. L., and Partridge, H., "Chemical-Kinetics Parameters of Hyperbolic Earth Entry," *J. Thermophysics and Heat Transfer* Vol. 15, 76-90 (2001).

[3] Losev, S. A., Makarov, V. N., Pogosbekyan, M. J., Shatalov, O .P., and Nikol'sky, V. S., "Thermo-chemical Nonequilibrium Kinetic Models in Strong Shock Waves of Air", AIAA Paper 94-1990 (1994).

[4] Bird, G. A., *Molecular Gas Dynamics and the Direct Simulations of Gas Flows*, Chap. 2, Clarendon, Oxford, England, U.K. (1994).

[5] Bird, G. A., "Monte-Carlo Simulation in an Engineering Context," *Rarefied Gas Dynamics*, edited by S. Fisher, Vol. 74, AIAA, New York, 239-255 (1981).

[6] Whiting, E. E., Park, C., Liu, Y., Arnold, J. O. and Patterson, J. A., "NEQAIR96, Nonequilibrium and Equilibrium Radiative Transport and Spectra Program: User's Manual", NASA Reference Publication 1389 (1996).

[7] Gryzinski, M., "Two-Particle Collisions. II. Coulomb Collisions in the Laboratory System of Coordinates", *Physical Review A*, Vol. 138, 322-334 (1995).

[8] Bourdon, A. Bultel, A. Panesi, M. and Magin, T., "Detailed and simplified kinetic schemes for high enthalpy air flows" in *Hypersonic Entry and Cruise Vehicles, VKI-LS Stanford, USA, June 30-July 3*, (2008).

[9] Hyun, S. Y., Park, C. and Chang, K. S., "Rate Parameters for Electronic Excitations of Diatomic Molecules, III. CN Radiation Behind a Shock Wave", AIAA Paper 2008-1276 (2008).

[10] Burke, P. G., "Electron-Atom, Electron-Ion, and Electron-Molecule Collisions", *Atomic, Molecular, and Optical Physics Handbook*, Drake, G. W. F., Editor, American Institute of Physics (New York), 536-554 (1996).

[11] Bray, I. and Stelbovics, A. T., "Convergent close-coupling calculations of electron-hydrogen scattering", *Physical Review A*, Vol. 46, 6995 – 7011 (1992).

[12] Bray, I., "Convergent close-coupling method for the calculation of electron scattering on hydrogenlike targets", *Physical Review A*, Vol. 49, 1066-1082 (1994).

[13] Fursa, D. V. and Bray, I., "Fully Relativistic Convergent Close-Coupling Method for Excitation and Ionization Processes in Electron Collisions with Atoms and Ions", *Physical Review Letters*, Vol. 100, 113201 (2008).

[14] Marchalant, P. and Bartschat, K., "R-matrix with pseudo-states calculation for electron-impact excitation and ionization of boron", *Journal of Physics B*, Vol. 30, 4373-4382 (1997).

[15] Zatsarinny, O., Bartschat, K., Bandurina, L. and Gedeon, V., "Electron-impact excitation of carbon", *Physical Review A*, Vol. 71, 042702 (2005).

[16] Burke, P. G. and Robb, W. D., "The R-matrix theory of atomic processes", *Advances in Atomic and Molecular Physics* Vol. 11, 143-214 (1975).

[17] Fischer, C. F., "Atomic Structure: Multiconfiguration Hartree-Fock Theories", *Atomic, Molecular, and Optical Physics Handbook*, Drake, G. W. F., Editor, American Institute of Physics (New York), 243-257 (1996).

[18] http://physics.nist.gov/PhysRefData/ASD/index.html

[19] Inokuti, M., "Inelastic Collisions of Fast Charged Particles with Atoms and Molecules – The Bethe Theory Revisited", *Reviews of Modern Physics* Vol.43, 297-343 (1971).

[20] Kim, Y.-K., "Scaling of plane-wave Born cross sections for electron-impact excitation of neutral atoms", *Physical Review A* Vol. 64, 032713 (20021.

[21] Wutte, D., Janev, R. K., Aumayr, F., Schneider, M., Schweinzer, J. Smith, J.J. and Winter, HP., "Cross Section for Collision Processes of Li Atoms Interacting with Electrons, Photons, Multiply Charged Ions, and Hydrogen Molecules", *Atomic Data and Nuclear Data Tables* Vol. 65, 155-180 (1997).

[22] Huo, W. M. and Kim, Y.-K., "Electron collision cross-section data for plasma modeling", *IEEE Transactions on Plasma Science*, Vol. 27, 1225-1240 (1999).

[23] Kim, Y.-K. and Rudd, M. E., "Binary-Encounter-Dipole Model for Electron-Impact ionization," *Physical Review A* Vol. 50, 3954-3967 (1994).

[24] http://Physics.nist.gov/PhysRefData/Ionization/index.html.

[25] Huo, W. M., "A convergent series representation of the generalized oscillator strength for electron-impact ionization and an improved Binary-Encounter Dipole model," *Physical Review* A, Vol. 64**,** 042719 (2001).

[26] Vriens, L., *Case Studies in Atomic Physics*, edited by E. W. McDaniel and M. R. C. McDowell, North-Holland, Amsterdam, Vol. 1, 335 (1969).

[27] Kim, Y.-K., "Scaling of Coulomb Born cross sections for electron-impact excitation of singly charged ions", *Physical Review A*, Vol. 65, 022705 (2002).

[28] Fischer, C. F., Tachiev, G., Gaigalas, G. and Godefroid, M. R., "An MCHF atomic-structure package for large-scale calculations", *Computer Physics Communications*, Vol. 176, 559-579 (2007).

[29] Kim, Y.-K. and Desclaux, J. P., "Ionization of carbon, nitrogen, and oxygen by electron impact," *Physical Rev*iew *A*, Vol. 66, 012708 (2002).

[30] Huo, W. M., "Electron-Impact Excitation and Ionization in Air", AIAA Paper 2008-1207 (2008).

[31] Brook, E., Harrison, M. F. A. and Smith, A. C., "Measurements of the electron impact ionization cross sections of He, C, O and N atoms", *Journal of Physics B*, Vol. 11, 3115 – 3132 (1978).

[32] Panesi, M., Magin, T. E., Bourdon, A., Bultel, A. and Chazot, O., "Analysis of the FIRE II Flight Experiment by means of a Collisional Radiative Model", AIAA Paper 2007-4023 (2007).

[33] Flannery, M. R., "Electron-Ion and Ion-Ion Recombination," *Atomic, Molecular, & Optical Physics Handbook*, edited by G. W. F. Drake, American Institute of Physics, Woodbury, New York, 1996 pp. 605-620. Note that the expression of the rate coefficient requires a normalization factor of $2/\pi^{1/2}$ to account for a normalized Boltzmann distribution

[34] http://amdpp.phys.strath.ac.uk/tamoc/DATA/RR/.

[35] Nahar, S. N. and Pradhan, A. K., "Electron-ion recombination rate coefficients, photoionization cross sections, and ionization fractions for astrophysically abundant elements. I. Carbon and nitrogen," *The Astrophysical Journal Supplement Series* Vol. 111, 339-355 (1997).

[36] http://amdpp.phys.strath.ac.uk/tamoc/DATA/DR/.

[37] Spence, D. and Burrow, P. D., "Cross sections for excitation of the $(2s^2 2p^2 3s)^4P$ and $(2s2p^4)^4P$ states of atomic nitrogen by near-threshold electron impact", *Journal of Physics B*, Vol. 13, 2809-2815 (1980).

[38] Doering, J. P. and Goembel, L., "Absolute differential and integral electron excitation cross sections for atomic nitrogen 1. The $^4S^o \rightarrow 3s\ ^4P$ (λ1200 Å) transition from 30 to 100 eV", *Journal of Geophysical Research*, Vol. 96, 16021-16024 (1991).

[39] Doering, J. P. and Goembel, L., "Absolute differential and integral electron excitation cross sections for atomic nitrogen 2. The $^4S^o \rightarrow 2p^4\ ^4P$ (λ1135 Å) transition from 30 to 100 eV", *Journal of Geophysical Research*, Vol. 97, 4295-4298 (1992).

[40] Yang, J. and Doering, J. P., "Absolute differential and integral electron excitation cross sections for atomic nitrogen 3. The $^4S^o \rightarrow {}^2D$ (λ5200 Å) transition from 5 to 30 eV", *Journal of Geophysical Research*, Vol. 101, 21765-21768 (1996).

[41] Tayal, S. S. and Beatty, C. A., "Oscillator strengths and electron-excitation cross sections for atomic nitrogen", *Physical Review A*, Vol. 59, 3622-3631 (1999).

[42] Frost, R. M., Awakowicz, P., Summers, H. P. and Badnell, N. R., "Calculated cross sections and measured rate coefficients for electron-impact excitation of neutral and singly ionized nitrogen", *Journal of Applied Physics*, Vol 84, 2989-3003 (1998).